Sustainability of aligned ZnO nanorods under dynamic shock-waves

M. Devika[1*], N. Koteeswara Reddy[2], V. Jayaram[3], K. P. J. Reddy[1]

[1]*Department of Aerospace Engineering, Indian Institute of Science, Bangalore 560012, India*
[2]*Center for Nanoscience and Engineering, Indian Institute of Science, Bangalore 560012, India*
[3]*Department of Solid-Sate and Structural Chemistry Unit, Indian Institute of Science, Bangalore 560012, India*

[*]Corresponding author, E-mail: devikareddy_81@rediffmail.com

Received: 26 April 2016, Revised: 14 August 2016 and Accepted: 30 October 2016

DOI: 10.5185/amlett.2017.6890
www.vbripress.com/aml

Abstract

In this article the sustainability of ZnO nanostructures under dynamic shock waves has been investigated. ZnO nanorods were synthesized on stainless steel (SS) substrates and exposed to shock waves in an inert atmosphere. The impact of shock waves on physical properties of ZnO nanostructures was analyzed. ZnO nanostructures grown on SS substrates exhibit excellent sustainability over different shock waves generated temperatures and pressures. The crystal structure and surface morphology of shock waves treated ZnO nanorods remain the same as untreated ones and however, the chemical stoichiometry and light emission properties are significantly changed. From these investigations it is emphasized that ZnO nanostructures could be adopted for various applications in space engineering technology where the surrounding temperature and pressure is below 8000 K and 2 MPa. Copyright © 2017 VBRI Press.

Keywords: ZnO nanostructures, dynamic shock waves, sustainability of nanostructures, solution growth, spray pyrolysis, chemical solution growth.

Introduction

Zinc oxide (ZnO), one of the wide band gap semiconductor materials, has received great attention in different fields of science and technology due to its unique physical, chemical and mechanical properties along with its eco-friendly, abundance and low-cost [**1**]. Practically ZnO has been successfully adopted in optoelectronics [**2**], piezoelectric devices [**3**, **4**], sensors [**5**], and solar cells [**6**, **7**] as an active material. Apart from these diverging applications, ZnO also evolved as a suitable candidate for various space engineering applications [**8**] due to its good radiation resistance, high thermal stability, and oxidation resistance even in harsh environments [**9**]. ZnO exhibits hardness of ~5 GPa and Young's modulus of ~111 GPa, which is comparable with the value of carbon nanotubes (~130 GPa) [**10-14**]. Further, ZnO exhibits a phase transition from wurtzite to rock salt (NaCl) structure at higher pressures, ~9.1 GPa [**15**], which is reversible at lower pressures [**16**] and thus, it retains the crystal structure as wurtzite.

Development of space shuttles (or spacecraft) is basically a multidisciplinary project and involves various departments. Among them, materials engineering is one of the crucial departments since each part of the shuttle (structures, thermal, propulsion, optics, power, equipment, and components) requires different characteristic materials. For example, thermally stable materials are required for thermal protection systems (TPS) to protect the vehicle from hostile environments (high enthalpy and high heat flux environments), sensors to detect the timely changes and thereby guide the vehicle, and devices to generate and store energy. Recent investigations on the role of materials (metals, organics, polymers, semiconductors, and insulators) in space engineering applications reveal that the properties of materials drastically degraded when exposed to space conditions. At present, therefore, low oxidation rate materials such as SiO_2, Al_2O_3, Cr_2O_3 or BeO are in use at below 1800 K and however, ZrB_2 and HFB_2 are explored up to 2000 K [**17**, **18]**.

In this direction Look *et al.* have studied the impact of high energy electrons (1-2 MeV) bombardment on the physical properties of ZnO crystals and revealed that ZnO is significantly more radiation resistive than that of other common semiconductor materials, such as Si, GaAs, CdS and GaN [**8**]. Besides this, various groups have studied the impact of rapid thermal annealing (RTA) on the physical properties of ZnO thin films as well as nanostructures up to the temperature of 1000 ^oC (1300 K) and noticed few interesting features. For example, Song *et al.* observed excellent improvement in the crystalline quality of ZnO films treated in RTA at 1000 ^oC for just 5 min under oxygen-rich environment [**19**]. Using similar approach Jang *et al.* obtained the best optical quality ZnO thin films by RTA treatment under Ar gas at 700 ^oC for

30 s [**20**]. Noticeably, compared to normal temperature and pressure, ZnO exhibits high permittivity, conductivity, and activation energy at higher temperatures (>1100 ^{o}C) [**21**]. In recent years, innovations in nanotechnology facilitate new pathways to solve various problems existing at micro and bulk levels [**22**]. In this concern, the nanostructures of ZnO material probably play a significant role in space engineering technology due to its typical physical, chemical and mechanical properties. Therefore, it is very crucial to understand the sustainability of ZnO nanostructures under harsh environments before the adoption in space engineering applications [**23**].

By keeping all these issues in mind along with the multifunctional device applications of ZnO, systematic investigations on ZnO nanostructures were initiated and explored the behavior of ZnO structures under dynamic shock waves, which generate high temperatures and pressures. For this, a homebuilt shock tube has been adopted, and the as-grown ZnO nanostructures were exposed to low enthalpy shock waves, as an initial step. In this paper we report the sustainability of ZnO nanostructures under harsh environments and impact on their physical properties. From these preliminary investigations it is emphasized that ZnO nanostructures are considerably stable under shock waves generated with temperatures and pressures upto 8000 K and 2 MPa.

Experimental procedure

ZnO nanostructures were synthesized on stainless steel substrates using a simple two-step process and exposed to shock waves. The as-grown and shock treated samples were characterized with advanced analytical techniques. All these issues are briefly described below in three sub-sections.

Materials

Steel substrates, zinc nitrate hexahydrate ($Zn(NO_3)_2$ $6H_2O$, Sigma-Aldrich, analytical grade), h*examethylenetetramine* ($C_6H_{12}N_4$, Sigma-Aldrich, analytical grade).

Synthesis of ZnO NRs

ZnO nanostructures were grown on ZnO seeded stainless steel substrates using well-established two-step process (seeding and growth). Initially, ZnO nanoparticles (NPs) films were deposited by following the procedure described elsewhere [**24**] with a thickness of about ~30-50 nm. In brief, 50 ml of zinc nitrate hexahydrate solution with 5 mM concentration was sprayed onto pre-heated SS substrates at 400 ^{o}C in pulse by using nitrogen as carrier gas. Here, the effective area of deposition was nearly about 5x5 cm^2. Further, the as-deposited ZnO NPs films were used as seed layers for the growth of ZnO nanorod structures (NRs) by chemical solution method, as described elsewhere [**25**]. In this case, an aqueous solution was prepared by dissolving zinc nitrate hexahydrate and h*examethylenetetramine* analytical grade chemicals in deionized water with an equimolar concentration of 10 mM. Then, the growth of ZnO NRs was carried out at 70 ^{o}C for 24 hrs.

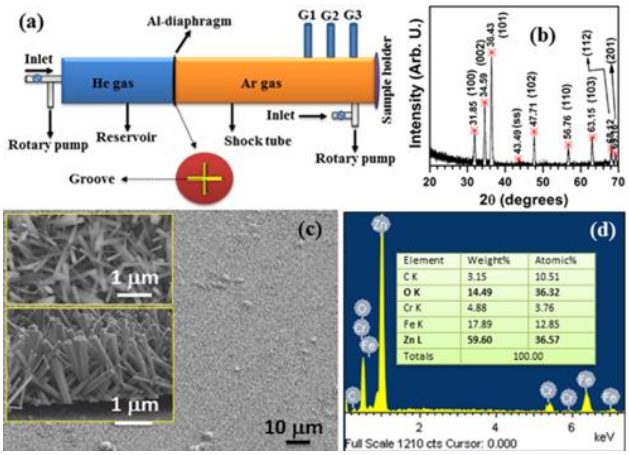

Fig. 1. (a) Schematic diagram of low enthalpy shock tube, (b) XRD profile, (c) Low magnification FESEM image (inset shows high magnification and cross sectional images), and (d) EDS profile (inset shows the quantified elemental composition) of as-grown ZnO NRs on stainless steel substrate.

Shock tube

Schematic diagram of the low enthalpy shock tube (LEST) is shown in **Fig. 1**. The shock tube consists of two sections: gas reservoir section (compression tube, blue in color) and test tube section (shock section, yellow in color). The pressure inside the tube, at each section, is measured with individual pressure gauges. The samples are fixed to sample holder at the end of the shock tube, and a thin aluminium diaphragm (black color ring) is fixed at the intersection of two sections. To evacuate both the sections, each section is individually connected to rotary pumps. In order to measure shock wave pressure, three individual piezoelectric pressure transducers are fixed at predetermined places and are connected to digital oscilloscope (supporting information, SI-1). In both the sections, once the pressure reduces to 10^{-2} mbar, initially the shock section is filled with test gas (present case high pure Argon) upto the required level (i.e. test gas pressure) and then, the compression tube is filled with helium gas. It abnormally increases the pressure in compression tube and ruptures the aluminium diaphragm, which produces the primary shock waves. These primary shock waves travel through shock tube and reflect at the end of the shock tube. In a short duration, enormous temperature and pressure is developed due to internal reflection of shock waves.

Characterization

The as-synthesized ZnO NRs on stainless steel substrates were cut into pieces (~1x1 cm^2) and exposed to dynamic shock waves generated in LEST. The untreated and shock waves treated ZnO NRs samples at four test gas pressures were considered as UT, T1 (low, i.e. 3000 Pa) and T4 (high, i.e. 11000 Pa). For all the experiments 3 mm thick aluminium diaphragms having a depth of 1/3" V shape

groove and a maximum driving gas pressure of ~5 MPa have been used. The sample(s) were fixed to the sample holder with stainless steel clamps and exposed to shock waves produced in a shock tube at different argon gas pressures varied from 3000 to 11000 Pa. Here, the whole sample was exposed to shock waves and therefore we assume the impact of shock waves on the sample is approximately uniform. The parameters related to shock waves like shock temperature, pressure, Mac number, and velocity were calculated using standard thermodynamic equations [**26]** (see SI-2) and the obtained data is given in **Table 1**.

Table 1. Evaluated parameters of shock waves developed in the shock tube.

Sample	Test gass (Ar) pressure (Pa)	Shock wave parameters			
		Temperature (K)	Pressure (MPa)	MAC No.	Velociry (km/s)
T1	3000	8100	1.18	5.98	1.92
T2	5000	7260	1.52	5.65	1.82
T3	8000	6120	1.68	5.18	1.67
T4	11000	5240	1.80	4.78	1.52

*MAC – ratio between speed of the object and velocity of the sound

The as-synthesized and shock wave treated ZnO NRs structures were examined with various advanced analytical techniques. The crystal-structure and phase purity of the structures was examined by X-ray diffractometer (XRD, Phillip's XPERT PRO, PANalytical B.V. The Netherlands)), transmission electron microscopy (TEM, FEI Tecnai T20 U), high resolution TEM (HRTEM), and selected area electron diffraction (SAED). The surface morphology and composition of the structures was estimated by field emission scanning electron microscopy (FESEM, ZEISS ULTRA 55, Gemini), energy dispersive X-ray spectroscopy (EDS, Oxford Instruments) attached with FESEM, and X-ray photoelectron spectroscopy (XPS, Axis Ultra 165). The impact of shock waves on the emission properties of structures was studied using mono-cathodoluminescence (CL, MONOCL4, Gatan) attached with FESEM.

Results and discussion

Shock wave characteristics

While increasing the test gas pressure from 3000 to 11000 Pa, the shock waves temperature decreased from 8100 to 5240 K, whereas the pressure developed in the shock tube slightly increased from 1.2 to 1.8 MPa. On the other hand, the velocity (Mach number, a ratio between shock waves and sound velocities) of shock waves decreased from 1.92 to 1.52 km s^{-1} (increased from 4.8 to 6) with the increase of test gas pressure.

Basic properties of ZnO NRs

ZnO nanostructures grown on stainless steel substrates by two-step process exhibit polycrystalline crystal structure **(Fig. 1b**) with pure hexagonal crystal phase since all the XRD peaks exactly matched with standard JCPDS data (Card No: 36-1451). However, the XRD peak diffracted at $2\theta = 36.43^{\circ}$ is more dominant as compared to other peaks. It indicates that most of the nanorods are preferentially oriented along the <101> direction. The full width at half maximum (FWHM) value of preferential peak is found to be 0.317°, which is nearly comparable with FWHM value (0.27°) of ZnO NRs grown by chemical vapor deposition method [**27]**.

FESEM analyses show that the as-grown structures have radial-growth pattern with partially overlapped morphology. These NRs are well covered on the whole substrate **(Fig. 1c)**. A possible reason for radial-growth of ZnO NRs is the mismatch between ZnO and stainless steel substrates (-10% and 35% along a- and c-direction; SI-3). The average length and diameter of ZnO NRs is found to be 2 μm and 120 nm, respectively. EDS analysis **(Fig. 1d)** reveals that the as-synthesized ZnO NRs have excellent chemical stoichiometry between its constituent elements since the Zn to O atomic% ratio is found to be 1.01. In addition to Zn and O peaks, we have noticed Fe and Cr sometimes Ni peaks, which belong to stainless steel substrate.

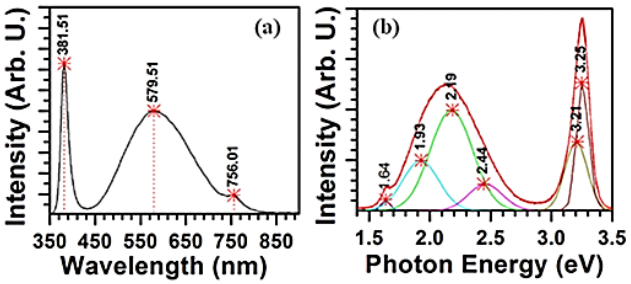

Fig. 2. (a) CL spectrum of ZnO NRs grown on stainless steel substrate and (b) its deconvoluted spectrum.

The CL spectrum of as-grown ZnO NRs **(Fig. 2a)** exhibit two strong emission peaks centered at wavelengths of 382 and 580 nm, and one weak peak at 756 nm. The sharp emission peak (382 nm = 3.25 eV) with FWHM of 100 meV belongs to ultra-violet (UV) near band edge emission of ZnO, whereas the broad band (BB) peak (580 nm = 2.14 eV) is attributed to various defect states present in the as-synthesized ZnO NRs. From the deconvoluted CL spectrum of ZnO NRs by Gaussian multi-peaks curve fit (**Fig. 2b**) it is found that the BB emission peak consists of three clearly distinguishable peaks centered at 1.93, 2.19 and 2.44 eV (642, 566 and 508 nm), whereas the sharp peak consists of one additional peak at around 3.21 eV (386 nm). It implies that the BB emission peak probably emerged due to the transition of excited carriers from conduction band to valance band (VB) via various defects states such as, as per the present results, zinc interstitials (Zn_I), zinc vacancies (V_{Zn}), and oxygen vacancies (V_o) (for more information see SI-4) [**28**, **29**]. Therefore, though the as-synthesized ZnO NRs are good in stoichiometry, crystallinity and phase purity, the structures consist of various defect states that were formed at the time of growth due to low temperatures and/or adsorption of

various chemical species (for example: OH^- or H_2O groups) from atmosphere. The figure of merit, defined as the relative CL peak intensity ratio of UV and BB peaks, i.e. I_{UV}/I_{BB}, of as-synthesized ZnO NRs is found to be 1.6 [**30**].

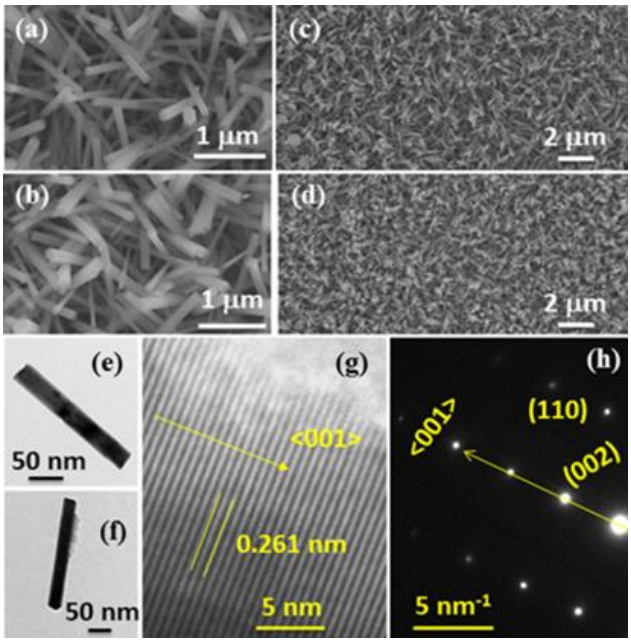

Fig. 3. High and low magnification FESEM images of shock wave treated ZnO NRs at (a & c) T1=3000 Pa, (b & d) T4=11000 Pa TG pressures, (e, f) bright field TEM images of untreated and treated ZnO NRs (T4=11000 Pa), (g) HRTEM, and (h) SAED images of untreated ZnO NR.

Sustainability of ZnO NRs under shock waves

After exposing ZnO nanostructures to dynamic shock waves produced at different TG pressures, the crystal structure, phase purity, and FWHM value of (101) peak (~0.315º) remain the same as untreated ZnO structures (SI-5a). However, the background of XRD spectra (see SI-5b) significantly increased with the decrease of TG pressure from 11000 to 3000 Pa. XRD spectrum of ZnO structures treated at 3000 Pa TG pressure consists of a strong background. The top-surface of ZnO nanorod structures **(Fig. 3)** also remains the same as untreated structures (see SI-1). However, a careful analysis of FESEM images reveals that the structures treated under shock waves exclusively consist of nanorods with uniform dimensions, most of larger size nanorods were absent (see SI-6). It indicates that a few of loosely bounded ZnO NRs with larger diameters probably gone-off due to the strong bombardment of high temperature and pressure shock waves. These analyses clearly emphasized that compared to untreated ZnO NRs structures, the structures treated at different TG pressures exclusively consist uniform NRs. As a result, the structures treated at 3000 Pa TG pressure consist of slightly less number of NRs than the structures treated at higher pressures. This could be the probable reason for the increase of substrate effect on the XRD spectra of ZnO NRs (SI-5a). These results reveal that the overall changes in crystal structure, morphology and even chemical composition are marginal. Therefore, the as-grown ZnO nanostructures on stainless steel substrates with overlapped morphology are significantly sustaining even under dynamic shock waves evolved with temperature and pressure of 8000 K and 2 MPa.

Changes in physical properties of ZnO NRs with shock waves exposure

In order to explore the changes in growth direction of ZnO NRs with shock waves treatment, all the nanostructures were sonicated into high pure ethanol solution and a few drops of solution were placed on carbon coated copper grid. The structures were dried under vacuum overnight and then, examined with TEM, HRTEM, and SAED. TEM studies show that the untreated and shock waves treated ZnO NRs consist of smooth surface morphology **(Fig. 3e and 3f)**. HRTEM analyses reveal that ZnO NR structures have single crystalline nature with a preferential growth along the (001) orientation since the calculated d-spacing value is about 0.261 nm **(Fig. 3g)**. The SAED studies also confirm that ZnO NRs are single crystalline and oriented along c-direction **(Fig. 3h)**. In addition to this, the SAED studies show that the (110) orientations are perpendicular to (001) orientations of ZnO. These observations are slightly different to the XRD results, which is probably attributed to the alignment of ZnO NRs [**31**].

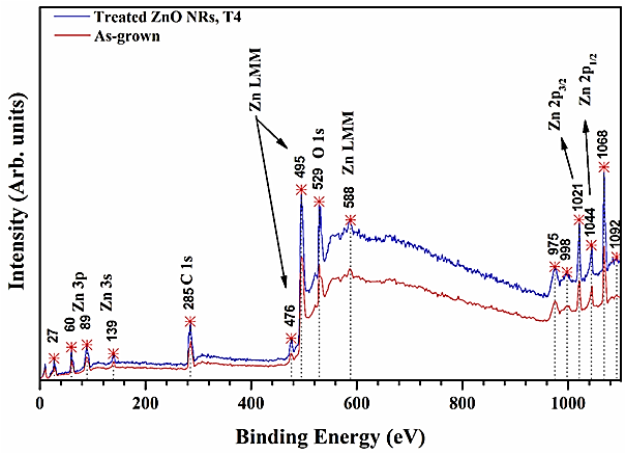

Fig. 4. XPS spectrum of untreated and treated ZnO NRs (T4=11000 Pa).

XPS spectrum of untreated and treated ZnO NRs at 11000 Pa TG pressure is shown in **Fig. 4** and all peaks are indexed with different states of Zn-O [**32**]. Here, the spectra were analyzed by calibrating the C1s peak to ~285 eV. Both the spectra consist of all most similar properties, except their intensities and sharpness **(Fig. 4)**. Noticeably, the shock waves treated ZnO NRs showed sharp and strong peaks than the untreated NRs. XPS peak centered at 529 eV belongs to oxygen bands (O 1s) in ZnO. XPS peaks centered at 1021 and 1044 eV belong to zinc bands (Zn 2p) in ZnO. From the analysis of high resolution profiles of O 1s and Zn 2p peaks (see SI-7) it is noticed that O 1s peak consists of an additional peak centered at 532 eV. This new peak belongs to oxygen in ZnOH or

adsorbed water molecules. Shock waves treated ZnO NRs exhibit slight improvement in the intensity of Zn as well as O peaks except 532 eV peak. While increasing, TG pressure the peak intensity of 532 eV peak decreased which indicates a significant reduction in the density of physisorbed chemical species present on the surfaces of NRs.

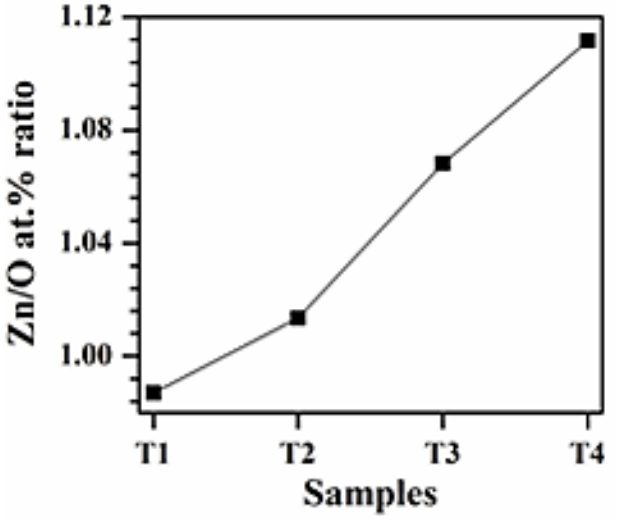

Fig. 5. Variation of Zn/O atomic% ratio of ZnO NRs with TG pressure.

From quantitative analysis of XPS spectra, elemental composition of Zn and O atoms were evaluated and variation of Zn/O atomic% ratio with TG pressure is shown in **Fig. 5**. As compared to EDS data, the Zn/O atomic% ratio of untreated ZnO NRs evaluated from XPS spectrum is slightly low (0.96), which suggests that the untreated ZnO NRs consist of oxygen-rich chemical composition. With the increase of TG pressure, oxygen content in the structures decreased and as a result, the atomic% ratio between Zn and O increased. It implies that ZnO nanostructures treated at higher TG pressures become Zn-rich (or oxygen deficient) in composition. The changes in the chemical composition of ZnO NRs with shock waves treatment can be described by considering the surface-texture of ZnO NRs. In general, ZnO NRs synthesized by hydrothermal method consist of various defects-states, present on surfaces. They adsorb different hydroxyl groups like OH^- ions and water molecules through weak electrostatic forces [**33**, **34**]. The physisorbed chemical species induce oxygen intercalated defect states (i.e. interstitial or vacancies) and thereby, degrade the overall quality of material by acting as recombination centers. Upon exposing the ZnO NR structures to shock waves, these physisorbed chemical groups vanished (or evaporated) due to a strong bombardment of shock waves with high temperature and pressure. It leads the overall oxygen content in ZnO NRs to lower values. While increasing the TG pressure, the impact of shock waves on ZnO NRs structures increased and as a result, the density of physisorbed chemical species decreased. Therefore, ZnO NRs exposed to shock waves produced at higher TG pressures consist of slightly Zn-rich chemical composition (Zn/O ~1.11).

CL emission spectrum of untreated and shock waves exposed ZnO NRs is shown in **Fig. 6a**. Upon exposing ZnO NRs to shock waves, the sharpness and intensity of UV peak increased and correspondingly the BB peak intensity decreased. These improvements in UV emission and reduction in BB peak intensity gradually increased with the increase of TG pressure. As a result, upon increase of TG pressure from 3000 to 11000 Pa, the figure of merit of ZnO NRs increased, **Fig. 6b**. Upon exposure of ZnO NRs to dynamic shock waves two different chemical modifications such as release of weakly adsorbed chemical species and nucleation of ionized atoms take place on ZnO NRs due to the presence of high temperature and pressure. Along with the release of physisorbed chemical species present on the surface of ZnO NRs, as described above, a short-while bombardment of high energetic shock waves probably induces the nucleation of unreacted Zn^{2+} and O^{2-} atoms, and leads the chemical composition of ZnO NRs to stoichiometric values [**35**]. As a result, the emission properties of ZnO NRs are significantly enhanced with their exposure to shock waves.

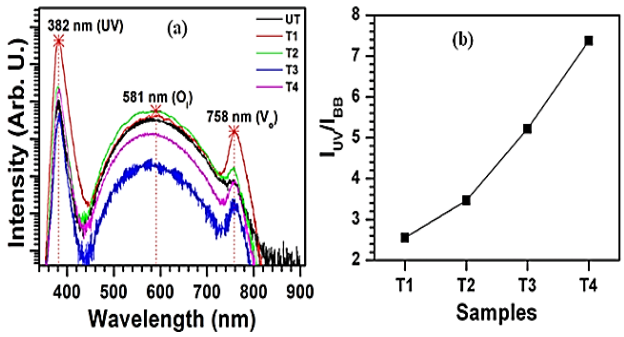

Fig. 6. (a) CL spectra of treated ZnO NRs at different test gas pressures (y axis is in log scale) and (b) I_{UV}/I_{BB} ratio of treated ZnO NRs at different TG pressures (T1-T4).

Conclusion

In view of typical properties of ZnO nanostructures**,** we have investigated the sustainability of partially overlapped ZnO NR structures under dynamic shock waves. ZnO NRs were synthesized on stainless steel substrates using spray pyrolysis and chemical solution methods. The structures were exposed to shock waves generated with high temperature upto 8000 K and pressure upto 2 MPa. The impact of shock waves on morphology, crystal structural and optical properties of ZnO nanostructures was investigated. From these studies, it is noticed that the morphology and crystal structure of shock waves treated ZnO NRs remain the same as untreated nanorods, whereas crystallinity and optical quality along with chemical stoichiometry are slightly improved. The overall results emphasize that the overlapped ZnO NRs grown on stainless steel substrates are stable up to the shock wave temperature of 8000 K and pressure of 2 MPa. Though the observed results are interesting, still more investigations have to be done particularly on the growth of NRs and shock wave impact at a specific area.

Acknowledgements

M. Devika wishes to acknowledge UGC for the sanction of Dr. D.S. Kothari Postdoctoral fellowship (No. F.4-2/2006(BSR)/13-703/2012(BSR)) and N. K. Reddy wishes to acknowledge CSIR for the sanction of Senior Research Associate ship under the scheme of Scientist's pool (No. 13(8525-A) 2011-Pool).

Author's contributions

MD and NKR performed all the experiments under the guidance of V. Jayaram and K P J Reddy. Manuscript was written by MD and NKR and corrected by VJ and KPJ.

Supporting information

A few details about instrumentation, experiemntal parameters, XRD details, FESEM and XPS data.

References

1. Ozgur U.; Alivov Y. I.; Liu C.; Teke A.; Reshchikov M. A.; Dogan S.; Avrutin V.; Cho S. J.; Morkoc H. *J. Appl. Phys.* **2005**, *98*, 041301.
2. Konenkamp R.; Word R. C.; Godinez M. *Nano Letters* **2005**, *5*, 2005.
3. Wang X. D.; Song JH, Liu J, Wang ZL *Science* **2007**, *316*,102.
4. Liu C.; Zhang W.; Sun J.; Wen J.; Yang Q.; Cuo H.; Ma X.; Zhang M. *Appl. Sur. Sci.*, **2014**, *322*, 95.
5. Tiwari, A.; Tiwari, A.(Eds), John Wiley & Sons, USA, **2012**.
6. Levy-Clement C.; Tena-Zaera R.; Ryan M. A.; Katty A.; Hodes G. *Advanced Materials* **2005**, *17*, 1512.
7. Chen X. -L.; Liu J. -M.; Ni J.; Zhao Y.; Zhang X. -D. *Appl. Sur. Sci.* **2015**, 328,193.
8. Look D. C.; Reynolds D. C.; Hemsky J. W.; Jones R. L.; Sizelove J. R. *Appl. Phys. Lett.* **1999**, *75*, 811.
9. Su B. Y.; Su Y. K.; Tseng Z. L.; Shih M. F.; Cheng C. Y.; Wu T. H.; Wu C. S.; Yeh J. J.; Ho P. Y.; Juang Y. D.; Chu S. Y. *J. Electrochem. Soc.* **2011**, *158*, H267.
10. Bradby J. E.; Kucheyev S. O.; Williams J. S.; Jagadish C.; Swain M. V.; Munroe P.; Phillips M. R. *Appl. Phys. Lett.* **2002**, *80*, 4537.
11. Kucheyev S. O.; Bradby J. E.; Williams J. S.; Jagadish C.; Swain M. V. *Appl. Phys. Lett.* **2002**, *80*, 956.
12. Yakobson B. I.; Smalley R. E. *Amer. Sci.* **1997**, *85*, 324.
13. Treacy M. M. J.; Ebbesen T. W.; Gibson J. M. *Nature* **1996**, *381*, 678.
14. Mondal, D.; Tiwari, A.(Eds), John Wiley & Sons, USA, **2012**.
15. Bates C. H.; Roy R.; White W. B. *Science* **1962**, *137*, 993.
16. Desgreniers S. *Phys. Rev. B* **1998**, *58*, 14102.
17. Opeka M. M.; Talmy I. G.; Zaykoski J. A. *J. Mater. Sci.* **2004**, *39*, 5887.
18. Wuchina E.; Opeka M.; Causey S.; Buesking K.; Spain J.; Cull A.; Routbort J.; Guitierrez-Mora F.; *J Mater. Sci.* **2004**, *39*, 5939.
19. Ashutosh Tiwari, Y.K. Mishra, H. Kobayashi, A.P.F. Turner (Eds), In the Intelligent Nanomaterials, 2nd Edition, John Wiley & Sons, USA, **2016**.
20. Jang Y. R.; Yoo K. H.; Park S. M. *J. Vacuum Sci. & Tech. A* **2010**, *28*, 216.
21. Thoria A. B. Egypt. J. Sol. **2007**, *30*, 13.
22. Koteeswara Reddy N.; Winkler S.; Koch N.; Pinna N. *ACS Applied Materials & Interfaces* **2016**, *8*, 3226.
23. Songjun Li, Yi Ge, Ashutosh Tiwari, Shunsheng Cao (Eds), In the A Temperature-Responsive Nanoreactor, WILEY-VCH Verlag, USA, **2010**.
24. Babu M. S.; Prashantha M.; Reddy N. K.; Ramesh K. *J. Nanoparticle Res.* **2013**, *15*, 1464.
25. Reddy N. K.; Ahsanulhaq Q.; Kim J. H.; Hahn Y. B. *Epl* **2008**, *81*, 38001.
26. Reddy K. P. J.; Hegde M. S.; Jayaram V.; Material processing and surface reaction studied in free piston driven shock tube, 26th Inter Symp on Shock Waves, Gottingen, Germany, Springer, **2007**, pp. 35.
27. Devika M.; Reddy N. K.; Kang J. W.; Park S. J.; Tu C. W. *Ecs Solid State Lett.* **2013**, *2*, P101.
28. Reddy N. K.; Devika M.; Shpaisman N.; Ben-Ishai M.; Patolsky F. *J. Mater. Chem.* **2011**, *21*, 3858.
29. Ahn C. H.; Kim Y. Y.; Kim D. C.; Mohanta S. K.; Cho H. K. *J. Appl. Phys.* **2009**, *105*, 013502.
30. Lin S. A. Z.; Hu H. L.; Zheng W. F.; Qu Y.; Lai F. C. *Nanoscale Res. Lett.* **2013**, *8*, 158.
31. Ahmed F.; Arshi N.; Anwar M. S.; Danish R.; Koo B. H. *RSC Advances* **2014**, *4*, 29249.
32. Kim J. W.; Kim H. B.; Kim D. K. *J. Korean Phys. Soc.* **2011**, *59*, 2349.
33. Capek, I. ; Tiwari, A.(Eds), Wiley and Sons, USA, **2015**.
34. Zhou H.; Alves H.; Hofmann D. M.; Meyer B. K.; Kaczmarczyk G.; Hoffmann A.; Thomsen C. *Physica Status Solidi B-Basic Res.* **2002**, *229*, 825.
35. Hsieh P. T.; Chen Y. C.; Kao K. S.; Wang C. M. *Appl. Phys. A-Mat. Sci. & Proc.* **2008**, *90*, 317.

Supplementary information

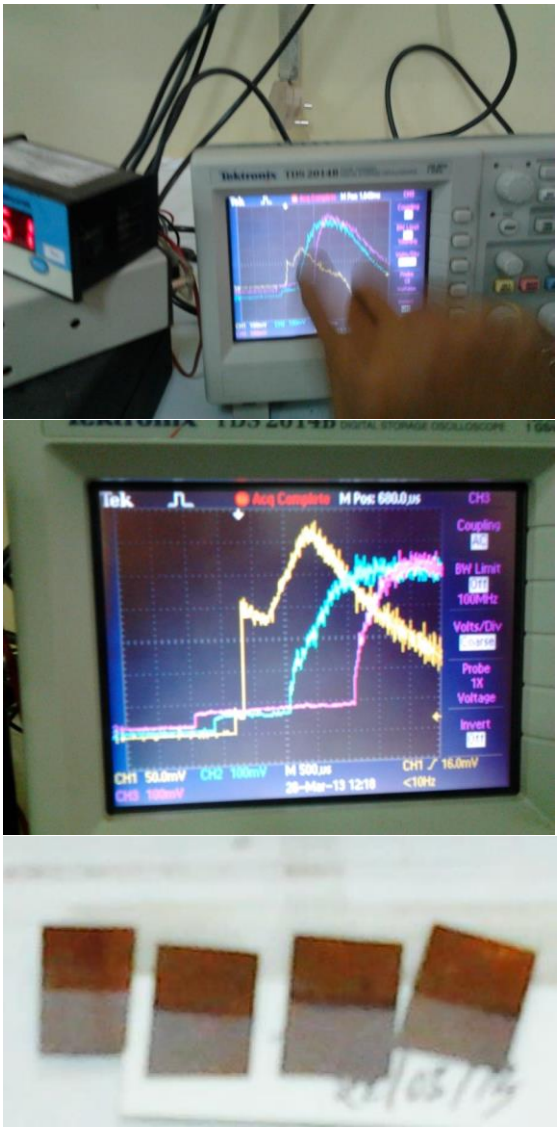

SI-1. Digital oscilloscope used for the measurements of pressure induced signals.

The properties of generated shock waves are calculated by evaluating the data obtained from parallely connected digital oscilloscope (Fig. S3) using the formulas given below.

Velocity of shock wave: $Vs = \Delta x/\Delta t$

where, Δx = distance between two pressure transducers (m); Δt = time interval to travel between two successive points (s)

MAC no: $Ms = Vs/a1$

where, a1 = speed of the sound in driven section = $\sqrt{(\gamma RT1)}$ here γ is specific heat in Ar (1.66), R is specific gas constant (208.13) and T1 is absolute temperature

Shock wave temperature = $[\{2(\gamma\text{-}1)\ Ms^2 + 3\gamma\}\{(3\gamma\text{-}1)\ Ms^2 - 2(\gamma\text{-}1)\}/(\gamma+1)^2\ Ms^2]\ T1$

Shock wave pressure = $\Delta P/1.025$ (psi); ΔP change in peak height.

SI-2. Equations used for the calculation of shock wave parameters.

ZnO hexagonal				(A2-Ao2)/(A2+Ao2)	Type of strain
	cub	a	3.249	-0.0998 (-9.98%)	Tensile strain since A<Ao
S S	3.5911	c	5.206	0.355 (35.52%)	Compressive strain since A>Ao
	Ao	A			

SI-3. Lattice mismatch between ZnO and SS substrate.

Here CB – conduction band, Zn_i and V_{zn} – zinc interstitials and vacancies, O_i and V_O – oxygen interstitials and vacancies, E_g – energy band gap, and VB – valance band.

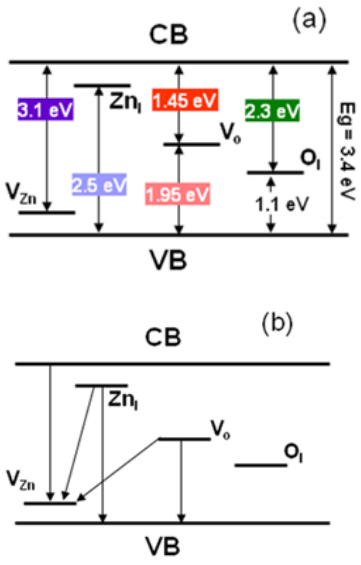

SI-4a. Schematic representation of energy level band diagram of ZnO with its impurity levels, respectively.

Gauss fit to Smoothed4_Book1E: Chi^2/D13842.56; R^21

Peak	Area	Center (eV)	FWHM (eV)	Height	Transitions
1	36	1.64	0.065	435	$V_o \rightarrow V_{Zn}$
2	738	1.93	0.296	1988	$V_o \rightarrow VB$
3	1733	2.19	0.347	3986	$Zn_I \rightarrow V_{Zn}$
4	366	2.44	0.278	1052	$Zn_I \rightarrow VB$
5	628	3.21	0.183	2743	$CB \rightarrow V_{Zn}$
6	**645**	**3.25**	**0.100**	**5142**	$CB \rightarrow VB$

Y offset = 0

SI-4b. Gaussian fit of CL spectrum for untreated ZnO nanostructures.

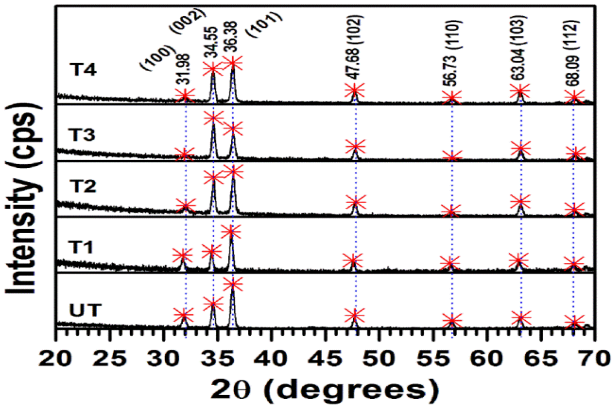

SI-5a. XRD profiles of shock wave treated ZnO NRs at different test gas pressures (UT- Untreated or pristine, T1=3000 Pa, T2=5000 Pa, T3=8000 Pa, and T4=11000 Pa).

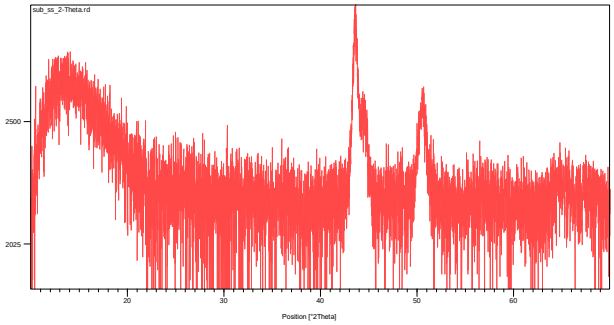

SI-5b. XRD profile of SS substrate.

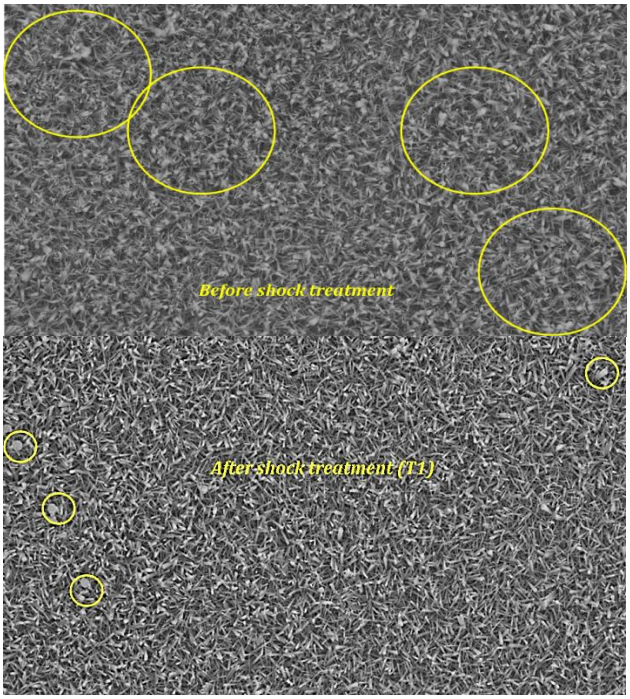

Keen observations reveal that most of the thicker ZnO NRs present on untreated samples are completely absent in treated samples.

SI-6. FESEM images of ZnO NRs before and after shock treatment (same magnification).

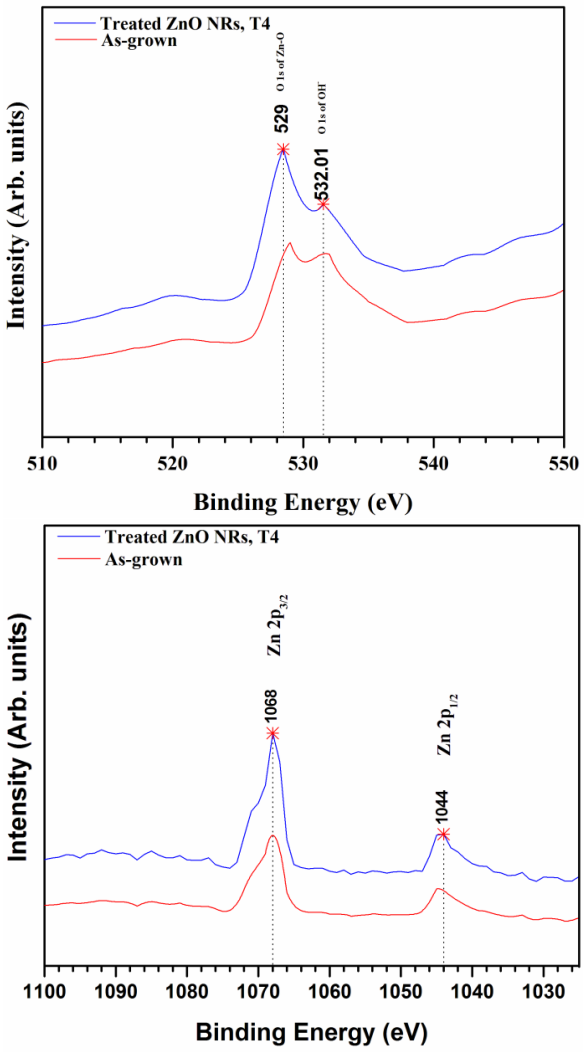

SI-7. O 1s and Zn 2p peaks of untreated and treated ZnO NRs.